Citation for published version:
Østgaard, N, Mezentsev, A, Marisaldi, M, Grove, JE, Quick, M, Christian, H, Cummer, S, Pazos, M, Pu, Y, Stanley, M, Sarria, D, Lang, T, Schultz, C, Blakeslee, R, Adams, I, Kroodsma, R, Heymsfield, G, Lehtinen, N, Ullaland, K, Yang, S, Qureshi, BH, Søndergaard, J, Husa, B, Walker, D, Shy, D, Bateman, M, Bitzer, P, Fullekrug, M, Cohen, M, Montanya, J, Younes, C, van der Velde, O, Krehbiel, P, Roncancio, JA, Lopez, JA, Urbani, M, Santos, A & Mach, D 2024, 'Flickering gamma-ray flashes, the missing link between gamma glows and TGFs', *Nature*, vol. 634, no. 8032, pp. 53-56. https://doi.org/10.1038/s41586-024-07893-0

DOI:
10.1038/s41586-024-07893-0

Publication date:
2024

Document Version
Peer reviewed version

Link to publication

This version of the article has been accepted for publication, after peer review (when applicable) and is subject to Springer Nature's AM terms of use, but is not the Version of Record and does not reflect post-acceptance improvements, or any corrections. The Version of Record is available online at:
http://dx.doi.org/10.1038/s41586-024-07893-0

University of Bath

Alternative formats
If you require this document in an alternative format, please contact:
openaccess@bath.ac.uk

General rights
Copyright and moral rights for the publications made accessible in the public portal are retained by the authors and/or other copyright owners and it is a condition of accessing publications that users recognise and abide by the legal requirements associated with these rights.

Take down policy
If you believe that this document breaches copyright please contact us providing details, and we will remove access to the work immediately and investigate your claim.

Download date: 14. May. 2025

Flickering Gamma Flashes – the Missing Link between Gamma Glows and Terrestrial Gamma-Ray Flashes

N. Østgaard[1], A. Mezentsev[1], M. Marisaldi[1], J. E. Grove[2], M. Quick[3], H. Christian[4], S. Cummer[5], M. Pazos[6], Y. Pu[5], M. Stanley[7], D. Sarria[1], T. Lang[3], C. Schultz[3], R. Blakeslee[3], I. Adams[8], R. Kroodsma[8], G. Heymsfield[8], N. Lehtinen[1], K. Ullaland[1], S. Yang[1], B. Hasan Qureshi[1], J. Søndergaard[1], B. Husa[1], D. Walker[4], D. Shy[2], M. Bateman[4], P. Bitzer[4], M. Fullekrug[9], M. Cohen[10], J. Montanya[11], C. Velosa[12], O. van der Velde[11], P. Krehbiel[7], J. A. Roncancio[11], J. A. Lopez[11], M. Urbani[11], A. Santos[12], D. Mach[13]

[1] Department of Physics and Technology, University of Bergen, Norway
[2] U.S. Naval Research Laboratory, Washington DC, USA
[3] NASA Marshall Space Flight Center, Huntsville, USA
[4] Department of Atmospheric Science, Earth System Science Center, University of Alabama in Huntsville, Huntsville, USA
[5] Duke University, USA
[6] Instituto de Ciencias de la Atmosfera y Cambio Climatico, UNAM, Mexico
[7] New Mexico Institute of Mining and Technology, USA
[8] NASA Goddard Space Flight Center, Greenbelt, USA.
[9] University of Bath, UK
[10] Georgia Institute of Technology, USA
[11] Polytechnic University of Catalonia, Spain
[12] Universidad Nacional de Colombia, Columbia
[13] Universities Space Research Association, Huntsville, Alabama, USA

*E-mail: Nikolai.Ostgaard@uib.no, orcid.org/0000-0002-2572-7033
**E-mail: Andrey.Mezentsev@uib.no, orcid.org/0000-0002-3471-7267
***E-mail: Martino.Marisaldi@uib.no, orcid.org/0000-0002-4000-3789

Two different hard radiation phenomena are known to originate from thunderclouds: Terrestrial Gamma-ray Flashes (TGF)[1] and gamma-ray glows[2]. Both share common underlying mechanism of avalanche of electrons accelerated to relativistic energies, but different production conditions lead to different phenomena. Glows are known to last for one-to-hundreds of seconds, have moderate intensities and originate from quasi-stationary thundercloud fields[2-5]. TGFs exhibit high intensities and have characteristic durations of tens-to-hundreds of microseconds[6-9]. TGFs often show close association with emission of strong radio signals[10-17] and optical pulses[18-21], which reveals involvement of lightning leaders in their generation.

Here we report a set of unique observations of a different type of gamma-ray events, which we call Flickering Gamma-ray Flashes (FGFs). FGFs in some ways resemble usual multi-pulse TGFs[22-24], but with larger number of pulses. However, each individual pulse has a longer duration compared to ordinary TGFs. Overall FGF durations span from 20 to 250 milliseconds, which reaches the lower boundary of the gamma-ray glow duration. All detected FGFs are radio and optically silent, which makes them distinct from normal lightning-related TGFs. An FGF starts as an ordinary gamma-ray glow, then suddenly increases exponentially in intensity, and turns into an unstable, "flickering" mode that produces a sequence of pulses. This phenomenon could be the missing link between the gamma-ray glows and conventional TGFs, whose absence has been puzzling atmospheric electricity community for two decades.

The unexpected detection of this remarkable class of gamma-ray event, Flickering Gamma-ray-Flashes (FGFs), was obtained during the ALOFT* aircraft campaign flying at 20 km altitude over thunderstorms in Caribbean and Central America in July 2023. For ALOFT, a NASA high-altitude aircraft was outfitted with an array of gamma-ray, optical, radio, and electric field instruments designed to study energetic emissions and lightning processes in thunderstorms (see Methods 2a).

One of two bright FGFs that was observed while passing over a gamma-glowing thundercloud[25] off the western coast of El Salvador is shown in Fig. 1A. This FGF has 17 pulses, of which 8 pulses (#2-9) are so bright that the large Bismuth-Germanate (BGO) gamma detector (225 cm^2) experienced saturation (Fig. 1A, inset), while the Lutetium Yttrium Orthosilicate (LYSO) detector (Fig. 1A, inset) was not saturated due to its much smaller detector area (1 cm^2) (see Methods 2a and 2b). The high fluence observed in both BGO and LYSO indicates clearly that the source radial distance to the foot-point was within 5 km range (see Methods 2a, 2e and 2f). The first pulses have durations and interpulse times of several milliseconds, then the intensity of the pulses increases and their duration decreases (down to 1-2 ms) until the pulse intensity decreases and separation between pulses becomes larger (up to 20 ms). The total duration of the FGF shown in Fig. 1 is ~50 ms.

* ALOFT: Airborne Lightning Observatory for FEGS and TGFs; FEGS: Fly's Eye GLM Simulator; GLM: Geostationary Lightning Mapper.

The Fly's Eye GLM Simulator (FEGS) onboard the aircraft did not show any optical signals of 337 nm and 777 nm emissions, related to streamers and leaders, (see Methods 2d) during the pulses of the FGF (Fig. 1B). The FEGS field-of-view (FOV) is 10 km x 10 km** square, significantly smaller than the UIB-BGO FOV, which is circular with ~20 km radius (see Methods 2a), but in this case the FGF source is well within the FEGS FOV (see Methods 2e).

The Electric Field Change Meter (EFCM) also on board the aircraft, which records close range Low Frequency (LF) electric field variations, shows no detectable signatures of electric activity during the pulses but a rather strong Narrow Bipolar Event (NBE) occurred 9 ms after the last pulse, followed by continuous lightning activity, as seen in both radio and optical data (Fig. 1B and Methods: Extended Data Fig. 1 and 4).

The ground-based LF radio data from the closest campaign radio receiver in Sisal, Mexico, 920 km away is shown in Fig. 1C and confirms that no radio signals that can be associated with the FGF pulses are seen, including the first few FGF pulses not captured by the EFCM. From this range, the background noise is equivalent in amplitude to lightning signals of very weak 1 kA peak current (see Methods 2c and Extended Data Fig. 2). Although there are numerous lightning pulses in the data window shown, most arrive at the sensor from a different direction than the known direction to the ER-2. The two axis orthogonal measurements are rotated so that a signal originating from that direction will have a large azimuthal B_φ (blue curve) component and a negligible radial B_r (red curve) component. The pulse at 12.474 seconds has a large B_r component and originates from a lightning source 725 km west of the ER-2 according to the Global Lightning Detection Network (GLD360). The NBE seen by EFCM was also seen in LF in Mexico (Fig. 1C).

FGFs were observed during five of ten total flights, each of which spent 2-3 hours above active gamma-glowing thunderclouds[25]. Fig. 2 shows all the 24 FGFs observed by the BGO detectors, with the in-Situ Thunderstorm Observer for Radiation Mechanisms (iSTORM) data overlaid for 21 of them. The count rates measured by iSTORM are about ½ to ⅔ of what BGO measures, consistent with the smaller detector geometric area (157 cm^2 versus 225 cm^2) and the smaller energy range (up to 5 MeV versus 30 MeV). The iSTORM data acquisition system is fully independent from that of the BGO. Despite some small differences (see Methods 2b), the two independent detector systems confirm that the FGF is a real phenomenon and cannot be a result of instrumental effects.

The FGFs were observed east of Yucatan, on the western coast of El Salvador, the coast of the Mexican states of Tabasco and Veracruz and on the east coast of Florida. All FGFs were observed over coastal regions and above gamma-glowing thunderclouds. The typical duration of the pulses is 1-2 millisecond, separated by 1-20 milliseconds, with the whole FGF lasting for tens to several hundreds of milliseconds. The FGFs typically start with a couple of less intense but longer (5-20 ms) pulses. Then a train of shorter (0.4-4 ms) intense pulses follows. Towards the end of the FGF the pulse intensity decreases and the separation between pulses becomes larger.

** +/- 5 km times +/- 5km from aircraft foot-point for cloud top at 15 km.

We have LF radio recordings for all 24 FGFs, EFCM for 3 of them, and optical data for 22 FGFs, and *no* detectable radio signals or optical pulses that could be associated with the pulses of the FGFs were observed. According to our observations, FGFs are both radio and optically silent (see Methods 2c and 2d), in contrast to normal lightning-related TGFs.

Multi-TGFs with a few pulses and associated radio signals have been observed by several spacecraft[22-24], but only BATSE[1] with its very large detector area (16000 cm^2) observed multi-TGFs that resemble the FGFs we report here. At the time they were identified and explained as just another type of TGFs[1, 26]. There have been a few modelling efforts that managed to reproduce the main features of the multi-TGFs observed by BATSE[27-28]. In these models the multi-TGF is initiated by a lightning discharge and the model also indicates that a new lightning discharge is likely to occur within microseconds of the last pulse of the multi-TGF. In these models the multi-TGF should be accompanied by significant charge moment changes and strong currents[27-28]. None of these features was observed during the FGFs we report here. Our observations show very clearly that there are *no* detectable radio signals, even when we are only 5-10 km away from the source, and there is *no* optical signal from any lightning leader, as should have been seen in the 777 nm and 337 nm bands.

Another remarkable feature is that in 10 of the 24 observations, the FGFs was followed by an NBE, not immediately (microseconds) after[28], but a few to tens of milliseconds after the last observed FGF pulse, followed by continuous lightning activity for hundreds of milliseconds, as seen in both radio and optical data (see Methods 2c and 2d and Extended Data Fig. 1 and 4).

During the ten flights of the campaign, we observed a total of 130 transient gamma-ray events: 24 FGFs, 96 TGFs and 10 glow bursts (< 100 ms) [25]. All of the TGFs and FGFs were observed when passing over gamma-glowing thunderclouds. Only a few of the TGFs (3 or 4) had intensities bright enough to be seen from space, which means that, at least in the Caribbean and Central America during summer, the thunderclouds produce almost 2 orders of magnitude more gamma flashes that can be detected from space and which questions the "rarity" of TGFs[29-30]. Our observations are consistent with those being obtained at the Telescope Array in Utah, which have detected a range of multi-pulse, weaker downward TGFs at the beginning of cloud-to-ground flashes[31].

Both TGFs and FGFs have a spectral shape that is expected from the Relativistic Runaway Electron Avalanche (RREA) process (see Methods 2e). This means that both phenomena require large potentials (hundreds of MV) and electric fields above the RREA threshold (280 kV/m surface equivalent) over large distances to accelerate electrons to relativistic energies and subsequently produce gamma photons with energies up to 30 MeV. While the electrons in the TGFs are accelerated in the strong transient electric fields associated with lightning[10-14], the FGFs reported here are *not* associated with the electric field of lightning discharges.

When optical measurements are available[18-21], TGFs are always associated with optical pulses simultaneous or slightly delayed to the TGF, while there are *no* optical pulses associated with the FGFs, indicating that leaders are involved in the generation of TGFs but not in FGFs. The TGFs also show close association with radio emissions[10-17], while there are *no* detectable radio signals (see Methods 2c) from FGFs.

Compared to gamma-ray glows, which are also radio and optically silent, the FGFs have much shorter duration and higher intensities. Similar to both TGFs and FGFs, the spectrum from gamma-ray glows also has the shape expected from the RREA process[32]. FGFs start as an ordinary gamma-ray glow, then experience sudden exponential increase, and turns into an unstable, "flickering", mode, falling into separate pulses.

Compared to TGFs the durations of the pulses in the FGFs are significantly longer (>1 ms) than that of the TGFs (~10-100 us) [6-9]. Scaling the flux values of TGFs seen from space down to 20 km altitude, we find that the brightest pulse in an FGF is just below the lower threshold that can be identified from space, consistent with the non-detection of FGFs by current space borne instruments[6-9] (see Methods 2e and 2f). The comparative characteristics of gamma-ray glows, FGFs and TGFs are summarized in Table 1.

Both observationally and phenomenologically the FGFs differ from both TGFs and gamma-ray glows, but carry features of both. Both in pulse duration and total duration and intensities, the FGFs fill the gap in the distribution of gamma emission phenomena from thunderclouds, between gamma-ray glows on one side and TGFs on the other side (Table 1). We therefore suggest that they can be the missing link between the two phenomena.

References

1 Fishman, G. J., Bhat, P. N., Mallozzi, R., Horack J. M., Koshut, J. M. et al. Discovery of Intense Gamma-Ray Flashes of Atmospheric Origin, *Science*, 264, 1313–1316, doi:10.1126/science.264.5163.1313 (1994).

2 Parks, G. K., Mauk, B. H., Spiger, R., & Chin, J. X-ray enhancements detected during thunderstorms and lightning activity. *Geophysical Research Letters*, 8(11), 1176–1179 (1981).

3 Eack, K. B., Beasley, W. H., Rust, W. D., Marshall, T. C., & Stolzenburg, M. Initial results from simultaneous observation of X-rays and electric fields in a thunderstorm. *Journal of Geophysical Research*, 101(D23), 29,637–29,640 (1996).

4 Østgaard, N , Christian, H. J., Grove, J. E. , Sarria, D., A. Mezentsev, A., et al. Gamma-ray glow observations at 20 km altitude. *Journal of Geophysical Research*, doi: 10.1029/2019JD030312, (2019).

5 Wada, Y., Matsumoto, T., Enoto, T., Nakazawa, K. , Yuasa, T., et al. Catalog of gamma-ray glows during four winter seasons in Japan. *Physical Review Research*, 3, 043117 doi: 10.1103/PhysRevResearch.3.043117 (2021).

6 Smith, D. M., Lopez, L. I. , Lin, R. P. and Barrington-Leigh, C. P., Terrestrial gamma-ray flashes observed up to 20 MeV, *Science*, 307(5712), 1085–1088, doi:10.1126/science.1107466 (2005).

7 Marisaldi, M., Fuschino, F., Labanti, C., Galli, M., Longo, F., et al. Detection of terrestrial gamma ray flashes up to 40 MeV by the AGILE satellite. *Journal of Geophysical Research*, 107, A00E13. https://doi.org/10.1029/2009JA014502 (2010).

8 Briggs, M. S., Fishman, G. J., Connaughton, V., Bhat, P. N., Paciesas, W. S., et al. First results on terrestrial gamma ray flashes from the Fermi Gamma-ray Burst Monitor. *Journal of Geophysical Research*, 115, A07323. https://doi.org/10.1029/2009JA015242 (2010).

9 N. Østgaard, N., T. Neubert, T., V. Reglero, V., K. Ullaland, K., S. Yang, S., et al. First ten months of TGF observations by ASIM. *Journal of Geophysical Research*. doi: 10.1029/2019JD031214, (2019).

10 Stanley, M. A., Shao, X.-M., Smith, D. M., Lopez, L. I., Pongratz, M. B., et al. A link between terrestrial gamma-ray flashes and intracloud lightning discharges. *Geophysical Research Letters*, 33, L06803. https://doi.org/10.1029/2005GL025537 (2006)

11 Cummer, S. A., Zhai, Y., Hu, W., Smith, D. M., Lopez, L. I., & Stanley, M. A. Measurements and implications of the relationship between lightning and terrestrial gamma ray flashes. *Geophysical Research Letters*, 32, L08811. https://doi.org/10.1029/2005GL022778 (2005).

12 Lu, G., Blakeslee, R. J., Li, J., Smith, D. M., Shao, X.-M., et al. Lightning mapping observation of a terrestrial gamma-ray flash. *Geophysical Research Letters*, 37, L11806. https://doi.org/10.1029/2010GL043494 (2010)

13 Shao, X.-M., Jacobsen, A. R., & Fitzgerald, T. J. Radio frequency radiation beam pattern of lightning return strokes: A revisit to theoretical analysis. *Journal of Geophysical Research*, 109, D19108. https://doi.org/10.1029/2004JD004612 (2004).

14 Cummer, S. A., Lu, G., Briggs, M. S., Connaughton, V., Xiong, S., Fishman, G. J., & Dwyer, J. R. The lightning–TGF relationship on microsecond timescales. *Geophysical Research Letters*, 38, L14810. https://doi.org/10.1029/2011GL048099 (2011).

15 Connaughton, V., Briggs, M. S., Xiong, S., Dwyer, J. R., Hutchins, M. L., et al. Radio signals from electron beams in terrestrial gamma ray flashes, *Journal of Geophysical Research*, 118, doi:10.1029/2012JA018288 (2013).

16 Cummer, S. A., Lyu, F., Briggs, M. S., Fitzpatrick, G., Roberts, O. J., & Dwyer, J. R. Lightning leader altitude progression in terrestrial gamma-ray flashes. *Geophysical Research Letters*, 42, 7792–7798. https://doi.org/10.1002/2015GL065228 (2015).

17 Dwyer, J. R., & Cummer, S. A. Radio emissions from terrestrial gamma-ray flashes. *Journal of Geophysical Research*, 118, 3769–3790. https://doi.org/10.1002/jgra.50188 (2013).

18 Østgaard, N., Gjesteland, T., Carlson, B. E., Collier, A. B., Cummer, et al. Simultaneous observations of optical lightning and terrestrial gamma ray flash from space. *Geophysical Research Letters*, 40, 2423–2426. https://doi.org/10.1002/grl.50466 (2013).

19 Neubert, T., Østgaard, N., Reglero, V., Chanrion, O., Heumesser, et al. A terrestrial gamma-ray flash and ionospheric ultraviolet emissions powered by lightning. *Science*, 367(6474), 183–186. https://doi.org/10.1126/science.aax3872 (2020).

20 Østgaard, N., Cummer, S. A., Mezentsev, A., Luque, A., J. Dwyer, J., et al. Simultaneous observations of EIP, TGF, Elve and optical lightnings. *Journal of Geophysical Research*, doi: 10.1029/2020JD033921, (2021).

21 Skeie, C. A., Østgaard, N., Mezentsev, A., Bjørge-Engeland, I., Marisaldi, M. et al. The temporal relationship between Terrestrial Gamma-ray flashes and associated optical pulses from lightning. *Journal of Geophysical Research*, doi: 10.1029/2022JD037128, (2022).

22 Mezentsev, A., Østgaard, N., Gjesteland, T., Albrechtsen, K., Marisaldi, M., et al. Radio emissions from double RHESSI TGFs. *Journal of Geophysical Research*, doi: 10.1002/2016JD025111, (2016).

23 Stanbro, M. C., Briggs, M. S., Roberts, O. J., Cramer, E. S., Cummer, S. A., & Grove, J. E. A study of consecutive terrestrial gamma-ray flashes using the Gamma-ray Burst Monitor. *Journal of Geophysical Research*, 123, 9634–9651. https://doi.org/10.1029/2018JA025710 (2018).

24 Mailyan, B., Stanbro, M., Briggs, M. S., Cummer, S., Dwyer, et al. Radio frequency emissions associated with multi-pulsed Terrestrial Gamma-ray Flashes. *Journal of Geophysical Research*, 126, e2020JA027928. https://doi.org/10.1029/2020JA027928 (2021).

25 Marisaldi, M., Østgaard, N., Lang, T., Sarria D., Mezentsev, A., et al. Tropical Thunderclouds Glow in Gamma Rays for Hours and over Thousands of Square Kilometers, *Nature Letter*, this edition (2024)

26 Nemiroff, R. J., Bonnell, J. T., Norris, J. P. Temporal and spectral characteristics of terrestrial gamma flashes, *Journal of Geophysical Research*, Vol. 102, No. A5, 9659-9665 (1997).

27 Dwyer, J. R., The relativistic feedback discharge model of terrestrial gamma ray flashes, *Journal of Geophysical Research*, 117, A02308, doi:10.1029/2011JA017160 (2012).

28 Liu, N. Y., and J. R. Dwyer, Modeling terrestrial gamma ray flashes produced by relativistic feedback discharges, *Journal of Geophysical Research*, 118, 2359–2376, doi:10.1002/jgra.50232 (2013).

29 Smith, D. M., Dwyer, J. R., Hazelton, B. J., Grefenstette, B. W., Martinez-McKinney, G. F. M., et al. The rarity of terrestrial gamma-ray flashes, *Geophysical Research Letters*, 38, L08807, doi:10.1029/2011GL046875 (2011).

30 Østgaard, N., Gjesteland, T., Hansen, R. S., Collier, A. B., Carlson, B. E. The true fluence distribution of terrestrial gamma flashes at satellite altitude. *Journal of Geophysical Research*, Vol. 117, A03327, doi:10.1029/2011JA017365, (2012).

31 Belz, J. W., Krehbiel, P. R.,Remington, J., Stanley, M. A.,Abbasi, R. U., LeVon, R., et al. Observations of the origin of downward terrestrial gamma-ray flashes. *Journal of Geophysical Research*, 125, e2019JD031940, doi: 10.1029/2019JD031940 (2020).

32 Sarria, D., Østgaard, N., Marisaldi, M., Lehtinen, N. G., Mezentsev, A., Library of simulated gamma-ray glows and application to previous airborne observations *Journal of Geophysical Research*, doi: 10.1029/2022JD037956, (2023).

Acknowledgements: This work made use of data from UIB-BGO, iSTORM, FEGS, EFCM, LF and VHF, GLD360. The ALOFT campaign and the UIB-BGO instrument was supported by European Research Council under the European Union's Seventh Framework Programme (FP7/2007–2013)/ERC grant agreement no. 320839 and the Research Council of Norway under contracts 223252/F50 (CoE) and contract 325582.
The use of the VHF data was supported by US NSF Grants 1720600 and 2214044.
– acknowledgement will follow……**(not finished)**

Author Contributions: N.O. and A.M. have led this study. The ALOFT campaign was led by N.O., T.L. M.M. and C.S. The UIB-BGO instrument was provided by N.O., M.M., K.U., S.Y. B.H.Q, J. S and B. H. and analyzed by N.O., M.M., D.S., N.L. The iSTORM data were provided and analyzed by J.E.G., D.S. and D. W. The FEGS data were provided by M.Q and the EFCM data were provided by H.C. and R. B. Radio data used in this study were provided and analyzed by S.C., Y.P. and M.P. and other LF stations were operated by P.B., M.F., M.C., J.M, C.V., O.vdV. J.A.R, J.A.L.,M.U. and A.S. The VHF data were provided and analyzed by M.S. and P.K. Radar data for the entire campaign were provided by I.A., R.K. and G.H.

Competing Interests: The authors declare that they have no competing financial interests.

Correspondence Correspondence and requests for materials should be addressed to N. Østgaard (Nikolai.Ostgaard@uib.no), A. Mezentsev (Andrey.Mezentsev@uib.no), and M. Marisaldi (Martino.Marisaldi@uib.no).

FIGURES AND TABLES

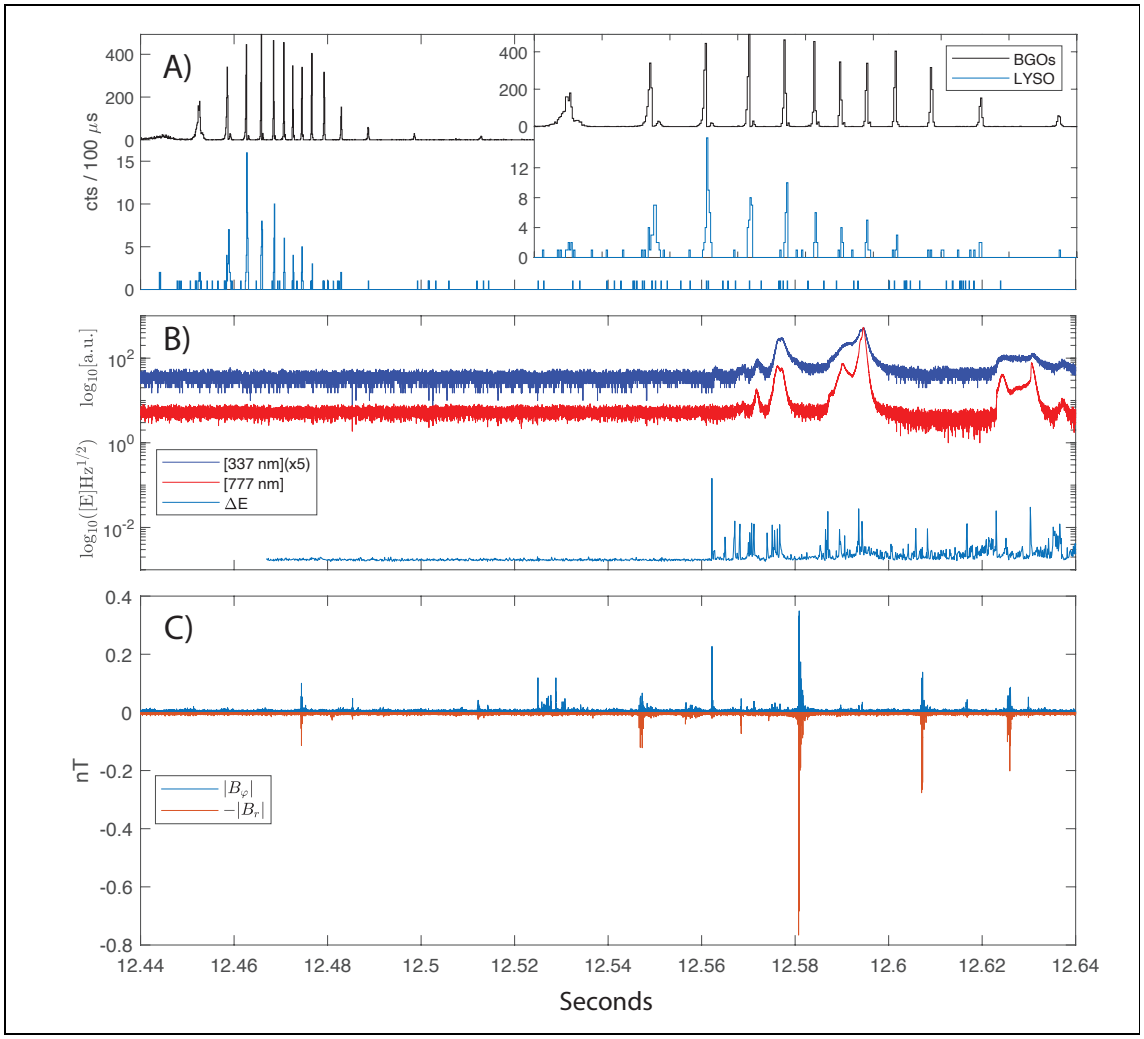

Fig. 1. Flickering Gamma-ray Flashes: 08.07. 2023: 05:01:12.44 UT - 05:01:12.64 UT. A) Gamma emissons measured by BGO and LYSO. The inset is zoomed in on the FGF time interval. B) FEGS optical emissions: 777 nm (red), 337 nm (blue) and EFCM: Electric field variability (ΔE), C) Low Frequency magnetic field radio emissions from Sisal, Mexico: radial (B_r) and azimuthal (B_φ) components.

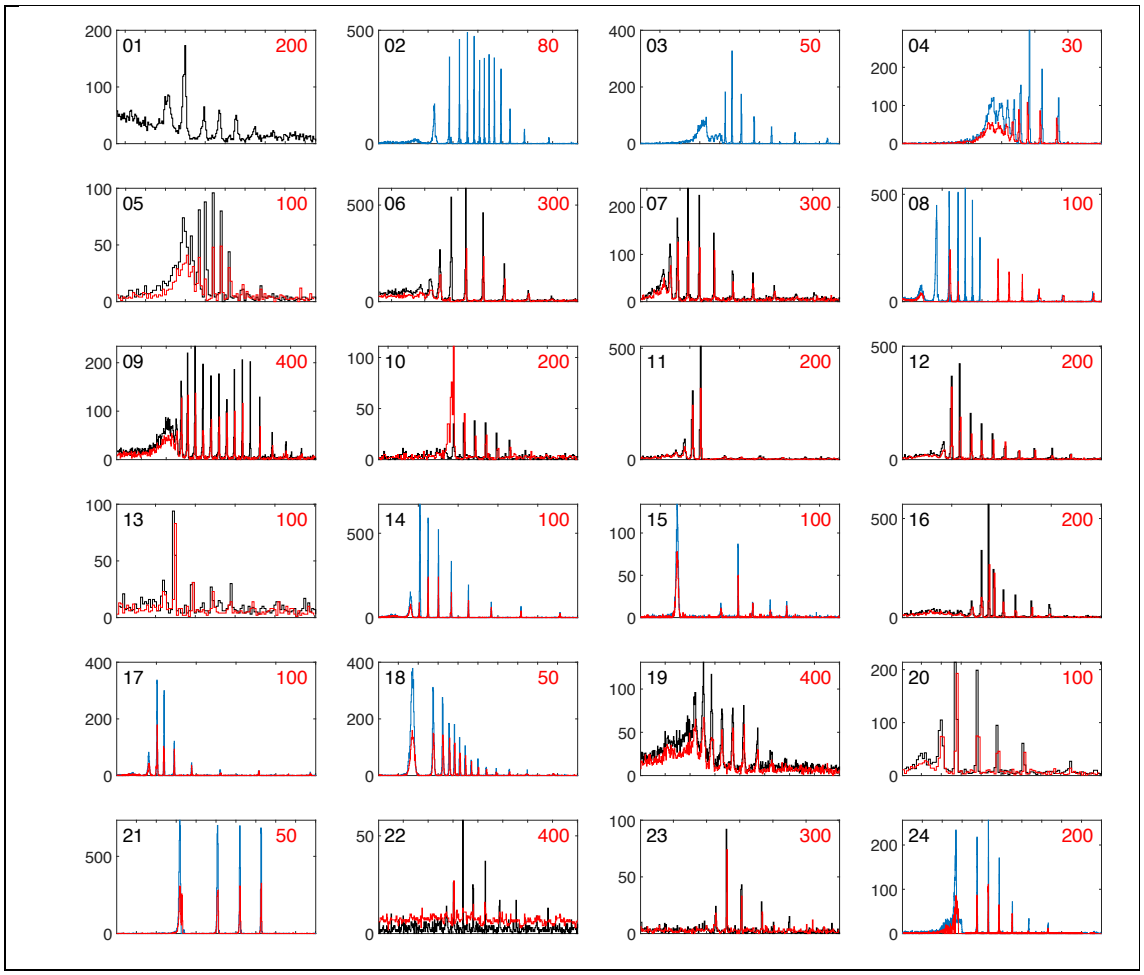

Fig. 2. Twenty-four FGFs seen by ALOFT. The BGO data are shown with black (cnts/1ms) and blue (cnts/100μs) and iSTORM data (for 21 of them) are overlaid in red with corresponding time bins. The values in the upper right corner (in red) are the time interval in millisecond shown in each plot. The numbering in the upper left corner corresponds to dates and times of each event and are given in Extended Data Table 5.

Table 1. Characteristics of glows, FGFs and TGFs observed at 20 km altitude.

Event	Event duration	Peak flux (cm^2 s $)^{-1}$	Optical	Radio	Spectra	Related to glows
Glow	1-100 s	[1] 2 -90	No	No	RREA[1]	Yes[1]
FGF total	10-100 ms	[2] $1.8 \times 10^2 - 2.3 \times 10^5$	No	No	RREA[1]	Yes[1]
TGF	10-1000 us	[3] $5.6 \times 10^5 - 10^8$	Yes[4]	Yes[5]	RREA[1]	Yes[1]

[1] From the ALOFT campaign.
[2] Max peak flux in BGO of single pulse in a FGF, when saturation is accounted for (see Methods 2f).
[3] ASIM TGFs mapped down to 20 km.
[4] When optical measurements are available.
[5] Some TGFs have no detectable radio.

METHODS

1. THE CAMPAIGN – OVERVIEW AND MISSION STRATEGY

During the month of July 2023 an aircraft campaign over thunderstorms in Caribbean and Central America with the NASA ER-2 aircraft was conducted; Airborne Lightning Observatory for FEGS* and TGFs (ALOFT). A total of ten flights (3-8 hours each) at 20 km altitude were performed. Each flight spent 3-4 hours above active thunderstorms.

The scientific target of the ALOFT campaign was to observe Terrestrial Gamma-ray Flashes (TGF) and gamma-ray glows from thunderstorms and the possible connection between the two. The aircraft was equipped with five independent gamma-ray detectors, 30 photometers, seven electric field sensors, two radars and two microwave radiometer systems. In addition, we had nine ground-based radio receivers operated during the campaign, covering Very Low Frequencies (VLF), Low Frequencies (LF) and two VHF Interferometers. The instruments used in this study will be described below.

Taking advantage of the novel mission concept, where one-second resolution data were downlinked in real-time, gamma-glowing clouds could be identified in real time, and the pilot was instructed to return to the same location as long as the thundercloud was glowing.

During these ten flights we observed a total of 130 transient gamma-ray events, 10 glow bursts (< 100 ms)[25], 96 TGFs and 24 Flickering Gamma-ray Flashes (FGFs), which we find to be a fundamentally different type of hard radiation from thunderclouds than the TGFs.

2. INSTRUMENTATION AND DATA ACQUISITION

a) Instrument description

The Bismuth-Germanate instrument from the University of Bergen (UIB-BGO). This instrument had four independent gamma detectors; one BGO detector, with three independent pairs of BGO scintillators read out by Photomultiplier Tubes (PMT) and three Lutetium Yttrium Orthosilicate (LYSO) detectors, all with fast readout electronics and with different geometric areas ranging from 0.09 cm^2 to 225 cm^2. From modelling work[33] it was expected that the count rate could increase by 4 orders of magnitude, depending on how close to the source the aircraft would be. Consequently, we designed our detectors to cover 4 orders of magnitude in count rates. The geometric areas, energy ranges and time resolutions for the four detectors are given in Extended Data Table 1. The three BGO/PMT detectors are similar to one of the four High Energy Detector modules of the Modular X- and Gamma-ray Sensor (MXGS)[34] that is flying on Atmosphere Space Interaction Monitor (ASIM) on the International Space Station (ISS). At 20 km altitude the BGO detectors are able to see events up to ~20 km radius from the foot-point of the aircraft[33]. The three BGO/PMT detectors and the medium LYSO/PMT detector share the same read-out electronics, while the two other LYSO/SiPM detectors have a separate read-out system.

* FEGS = Fly´s Eye GLM Simulator, GLM=Geostationary Lightning Mapper

The in-Situ Thunderstorm Observer for Radiation Mechanisms (iSTORM), is a gamma-ray spectrometer optimized to make sensitive measurements of bright, fast transients in the nuclear gamma-ray band (~300 keV to >5 MeV), designed and built by the US Naval Research Laboratory. The iSTORM instrument is a highly segmented array of fast, high-resolution inorganic scintillators. The large total geometric area (157 cm^2) provides high sensitivity, while the high segmentation and fast scintillation decay time preserves that large area for bright TGFs, which would paralyze a single detector of equal area. With slightly smaller detector geometric area (157 cm^2 versus 225 cm^2) and a smaller energy range (up to 5 MeV versus 30 MeV) the iSTORM sensitivity and range are slightly smaller than for the BGO. The specification of the iSTORM instrument is listed in Extended Data Table 2.

The Fly's Eye Geostationary Lightning Mapper (GLM) Simulator (FEGS), is an airborne array of multi-spectral radiometers optimized to measure the optical emission from lightning. These radiometers observe spectral emission from a variety of temperature regimes. The specification of FEGS is given in Extended Data Table 3. With 25 photometers centered at 780 nm FEGS provides images of the 777.4 nm emissions from lightning leaders over a nominal spatial footprint of 10 x 10 km^2 with a spatial resolution of 2 x 2 km^2 for cloud top at 15 km. The field-of-view (FOV) of the other photometers is 2 x 2 km^2 aligned with the center photometer of the 780 nm band. All photometers are sampled with a temporal resolution of 10 μs.

The Electric Field Change Meter (EFCM) is a two-channel (fast and slow) antenna that measures the derivative of the electric field impulse produced by lightning. The fast channel is designed to isolate the radiative component of the lightning discharge field while the slow channel is optimized to observe the electrostatic field component. The EFCM has multiple sensitivity ranges that are selectable during flight and samples with 16-bit resolution. Sample rate and decay time constant for EFCM are given in Extended Data Table 4. The EFCM is a triggered system.

The Low Frequency (LF) radio receivers in Mexico and Florida. The LF magnetic field radio emissions (30–300 kHz) were recorded in Sisal, Mexico (21.16°N latitude and -90.05°E longitude) and in Florida, USA (28.06°N latitude and -80.62°E longitude). The sensors have a flat frequency response from 100 to 200 kHz and a frequency-proportional response from 1 to 100 kHz. These sensors measure 2 orthogonal horizontal magnetic field components and thus also measure the direction of signal arrival. Absolute amplitude calibration was obtained from both laboratory measurements and in-field cross calibration with other magnetic sensors. The signals are sampled at 1 MS/s and GPS timing ensures absolute timing accuracy of better than 1 μs. The LF radio measurements are sensitive to electric current pulses with a time scale of 5 μs to 1 ms. The noise level varies somewhat in time due to anthropogenic sources, and the sensitivity to a fixed amplitude current pulse varies with distance to the signal source.

The Very High Frequency (VHF) Interferometer system was located at the University of Central Florida (UCF) Townes Institute Science and Technology Experimentation Facility (TISTEF) within the Kennedy Space Center, Florida (28.465163 deg N, -80.651996 deg E). VHF radio emissions of 1-160 MHz were recorded at 360 MHz from three sensitive inverted-V VHF antennas arranged in a near right triangle with

baseline lengths of 24.1, 25.4 and 33.4 meters. Electric field change waveforms obtained from a fast antenna (FA) having ~30 ns risetime and 100 microsecond decay time were simultaneously recorded with the VHF. Trigger lengths were typically 0.75 seconds in length with 0.25 seconds of pre-trigger before a triggering broadband VHF pulse.

b) Instrument performance of the gamma detectors

At 20 km altitude an aircraft can fly directly above the thundercloud and get close (<10 km) to the radiation source, so some of the FGFs (and a few TGFs) appeared so bright that some of our gamma-ray detectors saturated.

As shown in Fig. 1A and pointed out in the main text, the large BGO detector (225 cm^2) was saturated during the eight first pulses, while the smaller LYSO detector (1 cm^2) was not. The reason for this saturation is that the three BGO channels and the one LYSO channel each have a FIFO data buffer of depth 256, and the readout link speed for the 3 BGOs and LYSO altogether is around 330 kscdp/s (scdp: science data package of 48 bits). The link will loop around and read out one count at a time from every channel only if the FIFO of that channel is not empty. During a bright event of more than 256 counts (plus several extra count being read out at the same time) in a short period of time, the FIFO can be full and the following counts are discarded by the firmware until a new count is read out by the link (~75 kscdp/s), this gives the effect of a sudden drop of count rate to around 7.5 counts per 100 us. As seen in the inset of Fig. 1A, this drop is seen during the first eight pulses for BGO, but not in the LYSO data, which due to its much smaller detector area never reaches this count rate.

The iSTORM data acquisition system is fully independent from that of the BGO. iSTORM employs a commercial CAEN A5202 64-channel front-end electronics board intended for silicon photomultiplier (SiPM) readout of fast scintillators. The front-end board is controlled and read out by a BeagleBone® Black single-board computer (SBC). Data are read out in "Spectroscopy Mode," in which individual photons are logged by trigger number, time tag, and pulse height, and stored in flash memory. Inspection of the iSTORM data stream shows that the combined front-end board and SBC system is subject to regular busy times, including on 2-second and ~0.67-second periods, in which the system is unable to store events for durations of ~1 ms to ~10 ms. However, the trigger numbers of the stored events provide a direct measure of the number of triggers dropped during processor and front-end busy times, and it is therefore possible to calculate the total count rate, including triggers lost during these and other busy times. As configured for flights on 6 July and 8 July, iSTORM was particularly susceptible to noise and processor-induced deadtime and thus was not sensitive to the first three FGFs shown in Fig. 2.

As pointed out in the main text there are a few differences between the BGO data and the iSTORM data in Fig. 2.

For event #8 deadtime effects in the iSTORM are seen during the 1st, 5th and 6^{th} pulse, while BGO is not seeing the full signal for 7^{th}, 8^{th} and 9^{th} pulse. The deadtime effect of iSTORM is also seen in the 4^{th} pulse of event #6, 12^{th} pulse of #9 and 1^{st} pulse of #24.

For the event #10 the the BGO was saturated, and the first pulse appears as two separate pulses, while iSTORM shows clearly that this is indeed one large pulse.

Despite of these differences, the two independent detector systems confirm that the pulses we see are real and cannot be the result of instrumental effects.

c) No detectable electrical signals or radio signals from FGFs

EFCM on ER-2

For the 24 FGFs we have EFCM recordings for 3 of them, LF recordings from Mexico and Florida for all of them and VHF from Florida for the last one (#24).

Extended Data Fig. 1 shows three FGFs with synchronous EFCM recordings. Since this is a triggered system the EFCM data do not cover the first pulses of the FGF (Extended Data Fig. 1A and 1C). Counts from all three BGO detectors are binned into 100 μs bins to form the FGF light curves (black lines) with individual pulses clearly visible to the very end of each FGF event. Red lines show electric field variability which was calculated by finding logarithmic mean of the spectral amplitudes for each 100 μs time bin of the signal, such that the final variability is given by:

$$\Delta E = 10^{M},$$

$$M = \frac{1}{N}\sum_{k=1}^{N} \log_{10} S_k,$$

where S_k are power spectral density amplitudes for the whole frequency range up to 5 MHz sampled with a step of 10 kHz (each time bin was 100 μs).

Extended Data Fig. 1 clearly shows the absence of a noticeable radio signal during the three FGF events. At the same time, in all events radio recordings show a strong NBE signals (marked with black text and arrows) at about 10 ms after the final pulse of the FGFs (marked with red arrows). Those NBEs start long lasting (hundreds of milliseconds) periods of electromagnetic activity, which can be seen in each red curve after the NBE.

LF from Mexico and Florida

Performance details for these sensors are described in Section 2a. Signals during all 24 FGFs from the campaign were recorded by multiple sensors. The closest sensors were either Sisal, Mexico, or Melbourne, Florida. In all cases, there was no detectable signal above the noise floor during the time of the FGFs that originated near the FGF location.

The noise floor of the recorded signals enables us to establish an upper bound on the strength of any radio emissions associated with the FGFs. In the Extended Data Fig. 2 we show instantaneous LF magnetic field power for the horizontal magnetic field component maximized for the direction to the FGF location. Lightning pulses that

arrive from directions deviating by more than 20° in azimuth from the FGF location are masked out because these cannot be associated with the FGF.

To create a meaningful measure of sensitivity, we determine the expected amplitude of sources with known peak current values by establishing a correlation between the peak currents reported by the National Lightning Detection Network (NLDN) and the peak fields measured by the LF sensor for a source of known distance away. As an illustration, when examining the FGF located 75 km away from the sensor, we measure the peak LF fields of NLDN-reported events measured at the same distance (75-76 km) from the source. For a specific peak current value, a range of peak fields that span approximately a factor of 2 are found, and we utilize the median value as a representative measure for the equivalent field of that peak current.

Extended Data Fig. 2 shows the measured LF signal power during the time window of two FGF events. The first is the event analyzed in the main text from 2023/07/08 05:01:12 UTC (Extended Data Fig. 2A). The closest LF signal was measured in Sisal at 922 km distance. The background noise level shows that any FGF-associated radio signal would have to be from a source smaller than approximately 1 kA equivalent peak current. The second event is from 2023/07/29 21:03:19 UTC (Extended Data Fig. 2B). The closest LF signal was measured in Melbourne at 75 km distance. This is the FGF with the shortest distance to one of our LF sensors and thus the highest sensitivity to small signals. The background noise level shows that any FGF-associated radio signal would have to be from a source at least 10 times smaller than 1 kA peak current.

These measurements establish a strong upper bound on any possible LF radio emissions associated with FGFs. They confirm that the FGFs initiate and develop in the absence of any typical lightning flash processes.

VHF and FA from Florida

VHF source azimuths as mapped by the interferometer within a 200-millisecond interval around the time of the FGF are shown in Extended Data Fig. 3A with raw data superimposed and the FGF shown in Extended Data Fig. 3B. The signals seen at the two azimuth angles are ~30 km away from the receiver, which means that the signals coming from ~320° azimuth are ~5 km horizontal distance from the ER-2 location. There is activity from a storm about 40 km south of the ER-2 location (~250° azimuth), but no VHF sources are detected from the storm near the ER-2 (~320° azimuth), during the time of the FGF, consistent with the interferometer's FA waveform being silent, as well as the EFCM (Extended Data Fig. 1, lower panel) and LF (Extended Data Fig. 2B) measurements for this event. An NBE and subsequent IC flash from that storm is detected 14.5 ms after the last FGF pulse.

d) No detectable optical signals from FGFs

We have optical measurements by the FEGS, on board the aircraft for 22 of the of the 24 FGFs. The channels that are most sensitive to lightning activity, are the

25 photometers centered at 780 nm and one photometer centered at 340 nm. These two channels measure the 777.4 nm emission line from atomic Oxygen (OI) formed by disassociated molecular Oxygen in the hot leader channel, and the 337.1 nm emission line from and molecular Nitrogen ($N_2$2P) from colder streamer ionization waves.

Extended Data Fig. 4 shows all the FGFs and the accumulated optical signals from 777.4 nm emissions (red) and 337.1 nm emissions for 22 of the events. For events #20 and #21 the FEGS instrument was not working. The negative slopes that are seen in some of the panels are due to undershoot in the FEGS signals after pulses.

All the panels, except two, show that there is no optical activity within the FOV of the FEGS during the FGFs. In event #1 there are a few small optical pulses (seen as steps) which are not correlated in time with the pulses of the FGF (up to 10 ms delayed) and are likely from a different location than the FGF. The weak optical signals in event #5 that start before the FGF do not show any pulsed features and are most likely unrelated to the FGF.

The FOV of FEGS is 10 km x 10 km (5-7 km to the corners/sides for a cloud top at 15 km), but can see scattered light from at least 10 km from aircraft foot-point. Although the sensitivity of BGO falls off drastically from foot-point to 20 km horizontal distance (4 orders of magnitude)[32], strong signals from 20 km will still appear as weak signals above the noise level. However, more than half of the FGFs have intensities that indicate a source less than 5 km from foot-point and well within the FEGS FOV, and we do not see any optical signals for any of them.

For the weaker FGFs (9 total) we cannot exclude that the gamma source is more than 10 km away and therefore any light associated with them would not be seen by FEGS, but it is quite unlikely that this should occur for all of them.

e) Spectral characteristics and fluence estimates

In Extended Data Fig. 5 the spectral characteristics of two of the FGFs are shown. From the BGO instrument, which covers energies from 300 keV to >30 MeV, these two FGFs are among the brightest we observed and have sufficient count statistics to identify the shape of their energy spectrum and make an estimate of the fluence at source.

All the observed spectra are expected to come from the Relativistic Runaway Electron Avalanche (RREA) process. To assess if a typical RREA spectrum is detected, we used the GEANT4 software[35], that enabled us to simulate photon, electron, and positron propagation in any medium (here: the atmosphere, the detectors and surrounding structures). We tested a classical RREA photon spectrum of 1/E * exp (-E/7.3 MeV) up to 40 MeV at source, and a simple power law 1/E, which would be just an enhancement of the background spectrum, termed Modification of Spectrum (MOS) [36].

To perform the spectral analysis and find the best model fits, the following steps were performed; 1) Propagation, scattering and absorption of gamma photons in the atmosphere, as well as the production of secondary electrons and positrons, from 15 km altitude to the aircraft altitude at 20 km. 2) Energy Response Matrix of the BGO instrument, including scattering in the aircraft body, housing of the instrument and the other instruments in the aircraft pod located in the wing of the aircraft. 3) Maximum likelihood analysis to find the best parameter fits, using the same method as in ref.[37] based on the statistical approach presented by ref.[38]

The Extended Data Fig. 5 shows spectral fits for A) Event #2: 2023-07-08 at 05:01:12.451 UT. B) Event #9: 2023-07-24 at 06:56:07.270 UT. In both cases all the pulses, 17 (Fig. 1) and 16 (Fig. 3), respectively, are included. For both cases, the RREA model is a significantly better fit compared to the 1/E power law. This is shown by the Negative Log Likelihood values (NLL), where lower value means better fit. The NLL values for the model fits are listed in Extended Data Table 6. This demonstrates that a RREA process is the most likely explanation of the observed spectra. The spectral fits also give us the best fit radial distances (i.e. horizontal distance between the FGF source location and the aircraft). For these two FGFs the best radial distance is 3 km and 5 km, respectively, and gives support to our claim that the source of these bright FGFs is close to the aircraft foot-point. This estimate is for a source altitude at 15 km.

Combining all pulses for each event, we can estimate the number of source photons (above 400 keV) to be 1.5 x 10^{16} (event #2) and 7 x 10^{16} (event #9), assuming a source altitude at 15 km, which is used here as a reference altitude to compare with ASIM detections from the same assumed altitude. For event #9 half of these photons are from the first 50 ms long pulse, so the total number of photons for all the short 1-2 ms long pulses is on the order of 10^{16}, which would give about 10^{15} photons in each pulse at 15 km. We emphasize that these estimates are for the pulses in two of the brightest FGFs we observe. The majority of FGFs has lower fluence than these two. Of current spaceborne gamma detectors ASIM has the highest sensitivity and can identify gamma events with >5.6 x 10^{15} gamma photons (Table 1) from a source at 15 km within its trigger windows of 300μs, 1 ms, 3 ms or 20 ms. Pulses with ~10^{15} photons are just below the detection threshold of ASIM and are consistent with the non-detection of FGFs by any of the current spaceborne detectors (see Table 1 and Methods 1f).

f) Flux values for glows, FGFs and TGFs at 20 km from measurements

Here we explain how the flux values given in Table 1 for glows, FGFs and TGFs at 20 km altitude are obtained.

A glow is identified when the background of 2000 cnts/s increases by 25% (500 cnts/s), which then defines the lower flux limit for glows. The most intense glow we see is ~10 times the background (20 000 cnts/s). With a detector area of 225 cm^2 we get a range of 2 – 90 $(cm^2\ s)^{-1}$.

We have several FGFs where the BGO was saturated, but LYSO was not. This is the case for FGF #2, #8, #14 and #21, which are the four brightest FGFs we observe. Using the light-curve of the unsaturated LYSO we can estimate what the peak flux in BGO should have been. These estimates are listed in Extended Data Table 7, and the largest estimate we find is for 1st pulse in #21, where the measured flux should be increased to 5250 cnts/100μs (a factor of 7). The lowest maximum peak flux we observe during a FGF is the 3rd pulse of #10 (~40 cnts/ms). With a detector area of 225 cm^2 this gives us a range of 1.8 x 10^2 – 2.3 x 10^5 (cm^2 s)$^{-1}$.

For TGFs we will give the flux range based on the ASIM measurements mapped down to 20 km altitude, assuming production altitude at 15 km. The weakest TGF that can be identified in the ASIM data is ~10 cnts/ms and the brightest is ~1000 cnts/500μs. The ASIM MXGS HED detector area is ~900 cm^2. Combining the absorption from 20 km to 400 km (factor of 8 obtained from GEANT simulation) and the 1/r^2 effect (factor of 6400), the total scaling factor between 400 km and 20 km is ~50 000. Taking both the detector area and the total scaling factor into account we get a range of 5.6 x 10^5 - 10^8 (cm^2 s)$^{-1}$ for ASIM TGFs mapped down to 20 km. Only a few (3-4) of the 96 TGFs seen during the ALOFT campaign had fluxes above this lower limit and could have been seen from space. The brightest peak flux of a single pulse in the FGFs we observed (1st pulse of #21) is just below the lower threshold and would probably not been identified in data from any current spaceborne detectors.

EXTENDED DATA FIGURES AND TABLES

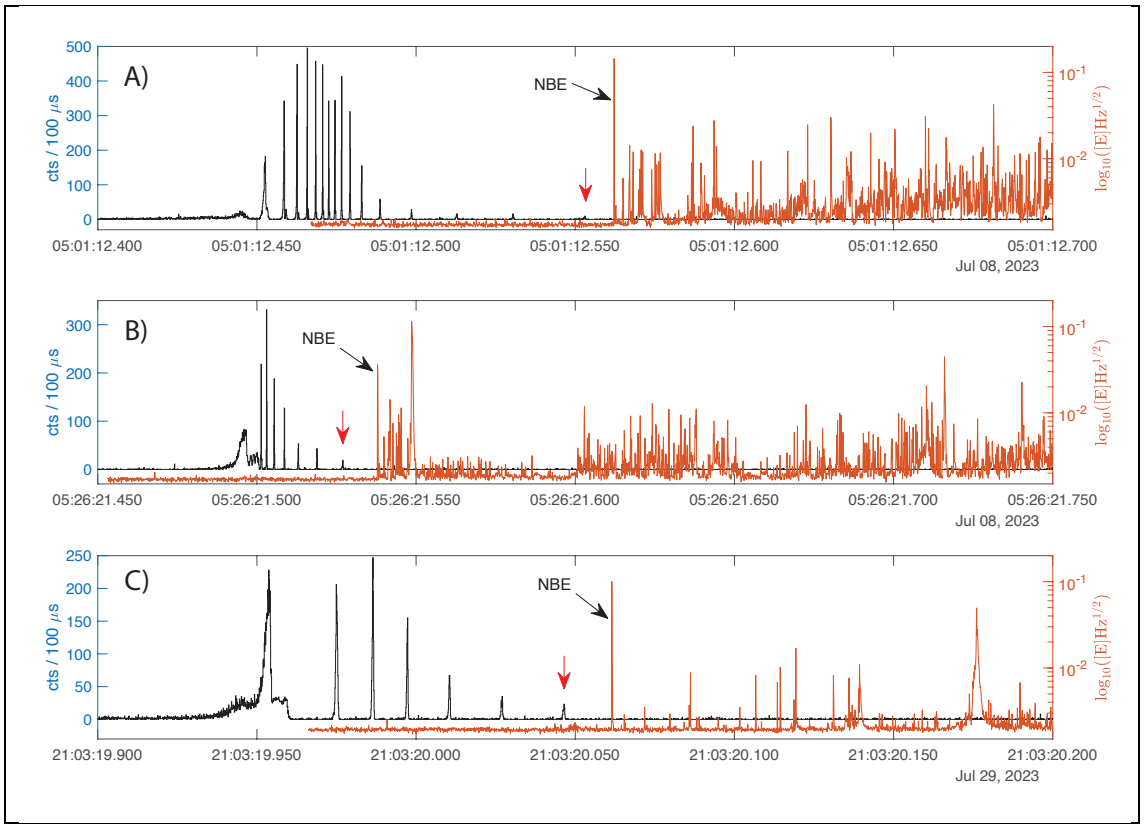

Extended Data Fig. 1. Three FGF events with EFCM recordings. Black lines show FGF light curves of the FGFs, while red lines represent electric field variability as recorded by EFCM. The last pulse of the FGF is marked with a red arrow and the following NBE with a black arrow.

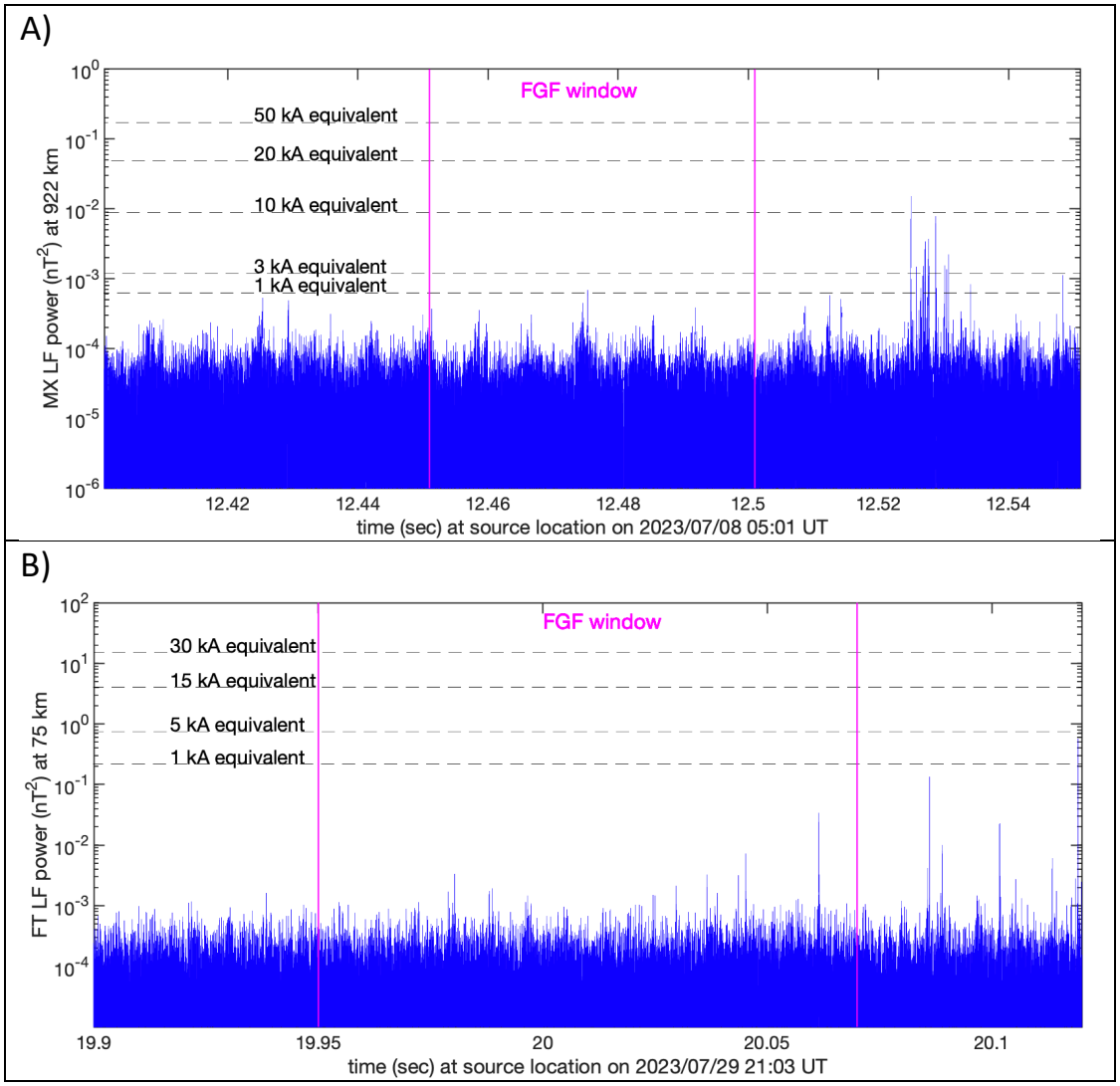

Extended Data Fig. 2. LF signal power during the time window of two FGF events. Overlaid are the data-derived peak power of lightning pulses at the observed distance for a range of peak currents. For the 2023/07/08 05:01:12 UTC FGF (panel A), the noise level and 922 km distance imply that any current pulses associated with the FGF must be lower than 1 kA equivalent. For the 2023/07/29 21:03:19 UTC FGF (panel B), the noise level and much shorter 75 km distance that any current pulses associated with the FGF must be at least 10 times smaller than 1 kA.

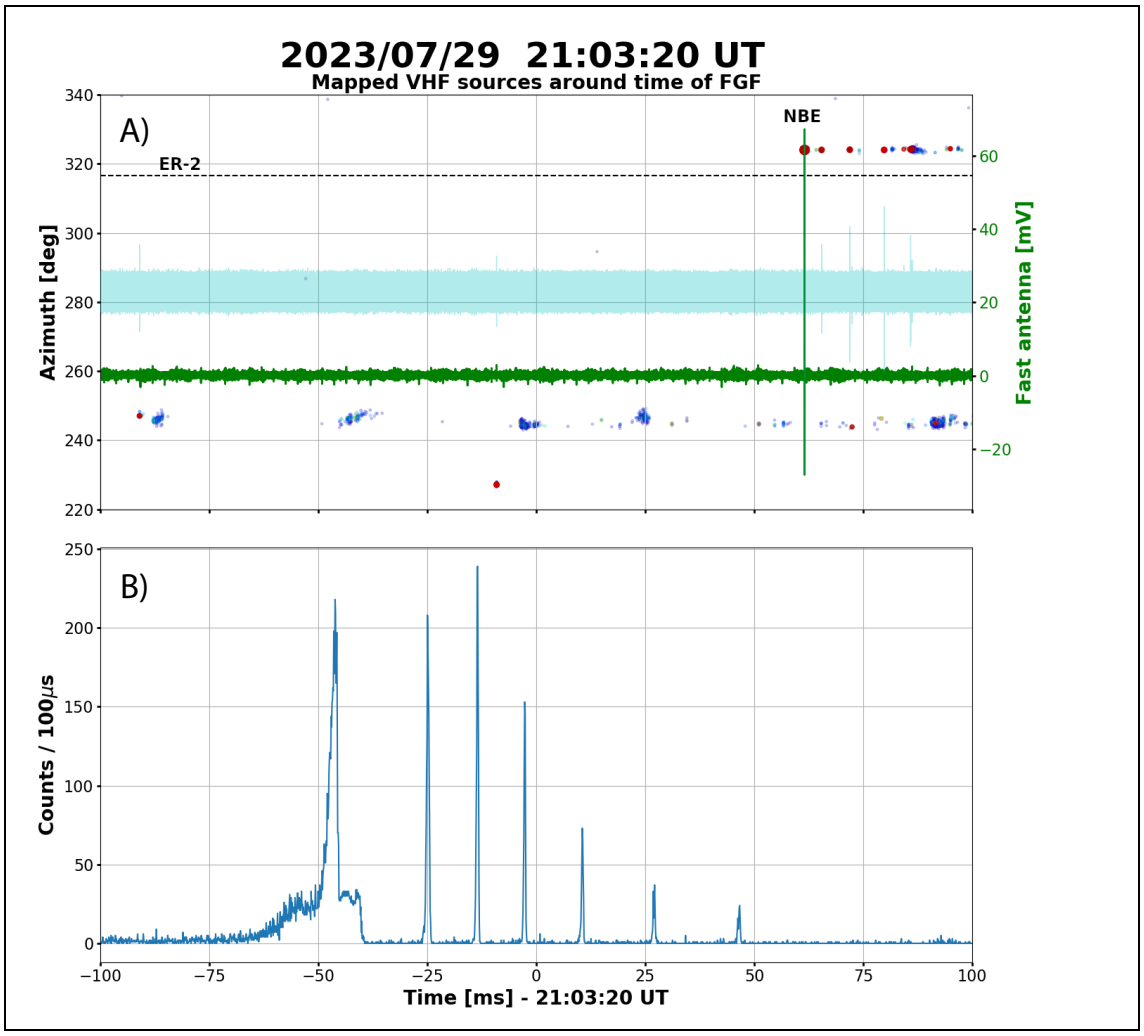

Extended Data Fig. 3. VHF and FA signals during the FGF on July 29, 2023. A): A 200-millisecond interval of VHF source azimuths with fast antenna data (green) and raw VHF data (cyan). Sources are color-coded according to VHF power ranging from dark blue (weakest) to bright red (strongest). The azimuth location of the ER-2 is marked with a dashed line. B): The BGO data in 100 microsecond bins.

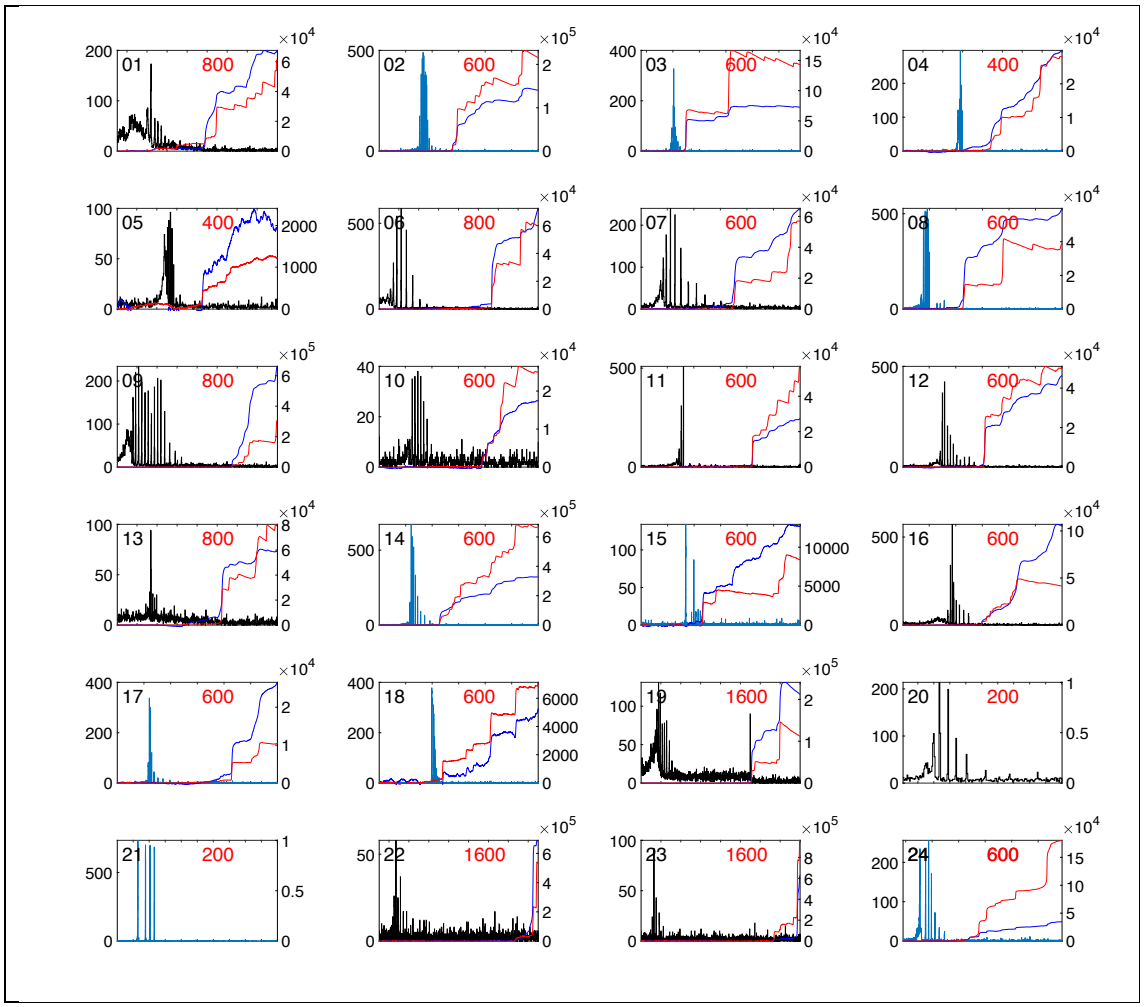

Extended Data Fig. 4. Optical measurements for 22 of the 24 FGFs. Black and blue curves are the FGFs with bins of cnts/ms and cnts/100μs, respectively. The accumulated optical signals are shown in red (777.4 nm emissions) and blue (337.1 nm emissions). For event #20 and #21 the FEGS instrument was not working.

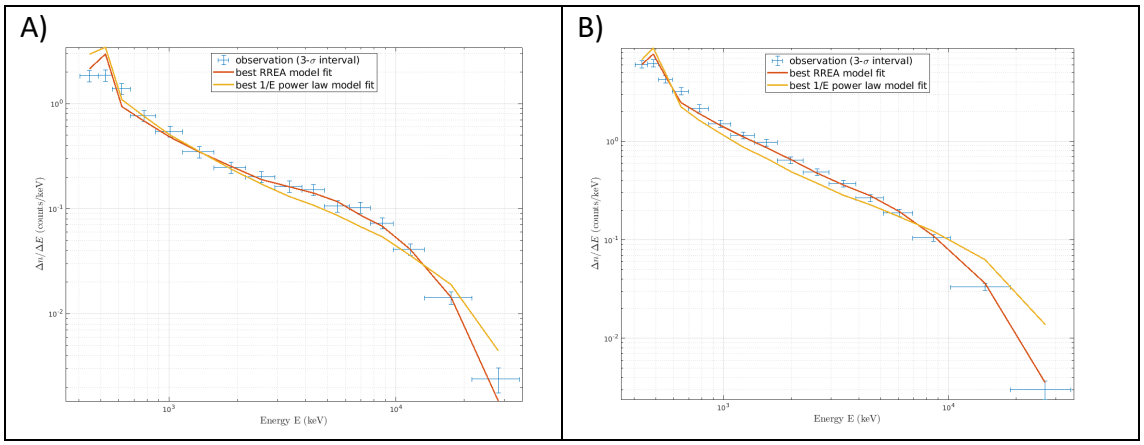

Extended Data Fig. 5. Spectral measurements and fits for two bright FGFs: A) #2 B) #9. Negative log-likelihood (NLL) values for the spectral fits are given in Extended Data Table 6.

Extended Data Table 1. Specification for the UIB-BGO detectors

Detector	Area (cm^2)	Energy range	Time resolution
BGO/PMT[1]	225	300 keV to > 30 MeV	28 ns
LYSO/SiPM[2]	25	1 MeV to >30 MeV	16 ns
LYSO/PMT[1]	1	>100 keV	28 ns
LYSO/SiPM[2]	0.09	>300 keV	16 ns

[1] Photo-Multiplier Tube.
[2] Silicon PhotoMultiplier (Data from these LYSO/SiPM detectors are not used in this paper).

Extended Data Table 2. Specification for the iSTORM detectors

Detector	Quantity	Size	Energy range	Time resolution
$CeBr_3$/SiPM	32	2.5Ø x 2.5 cm^{3*}	~300 keV – 5 MeV	<1 μs
Plastic/SiPM	1	1 x 1 x 1 cm^3	>100 keV	<1 μs
SiPM array	1	2.5Ø cm	n/a	<1 μs

* Total area of all $CeBr_3$ is 157 cm^2.

Extended Data Table 3. Specification for FEGS

Center Wavelength (nm)	Quantity	Emission (nm)	FWHM (nm)	Species
340[1]	1	337.1	10	N2
500[1]	1	500.5	10	NII
750[1]	1	Broadband (400-1100)	800	multiple
780[1]	25[2]	777.4	10	OI
870[1]	1	868.3	10	NI
1570[1]	1	multiple	130	NI

[1] All photometers have sample rate of 10 μs.
[2] Provides images of 10 x 10 km^2, with a spatial resolution of 2 x 2 km^2.

Extended Data Table 4. Specification for EFCM

Channel	Sample rate (MHz)	Decay time constant
Fast	10	100 μs
Slow	1	100 ms

Extended Data Table 5. Date, time and ER-2 location for the 24 FGF events

ID	Date	Time	Latitude	Longitude
01	2023-07-06	05:08:47.300	19.2000	-94.4382
02	2023-07-08	05:01:12.451	12.8908	-89.3482
03	2023-07-08	05:26:21.493	12.9497	-89.4361
04	2023-07-24	05:45:49.238	19.1567	-94.6887
05	2023-07-24	06:09:27.970	19.3632	-94.4779
06	2023-07-24	06:43:19.640	19.2486	-93.7970
07	2023-07-24	06:55:21.650	19.2618	-94.0376
08	2023-07-24	06:55:28.868	19.2721	-94.0474
09	2023-07-24	06:56:07.270	19.3268	-94.0992
10	2023-07-24	07:02:22.725	19.2813	-94.1986
11	2023-07-24	07:02:41.534	19.2739	-94.1643
12	2023-07-24	07:03:14.041	19.2610	-94.1062
13	2023-07-24	07:03:41.869	19.2501	-94.0569
14	2023-07-24	07:04:10.215	19.2387	-94.0061
15	2023-07-24	07:06:18.667	19.1862	-93.7735
16	2023-07-24	07:12:41.068	19.2708	-94.0431
17	2023-07-24	07:13:20.208	19.3299	-94.0921
18	2023-07-24	07:13:42.197	19.3624	-94.1190
19	2023-07-24	07:13:52.156	19.3769	-94.1310
20	2023-07-24	07:41:32.440	19.2368	-93.8473
21	2023-07-24	07:43:00.805	19.1793	-93.6992
22	2023-07-26	01:41:04.633	17.4054	-94.1734
23	2023-07-26	03:10:27.115	17.6995	-94.8623
24	2023-07-29	21:03:19.950	28.6903	-80.8939

Extended Data Table 6. Parameters for the spectral fit in Extended Data Fig. 3.

Spectral shape	NLL values – Extended Data Fig 3A	NLL values – Extended Data Fig 3B
RREA	2.9	5.8
Power law (1/E)	4.6	22.8

Extended Data Table 7. Estimated maximum peak flux of saturated pulses.

Saturated FGF pulses	Measured peak flux [cnts/100μs]	Saturation factor	Estimated peak flux when saturation is accounted for [cnts/100μs]
#2, 4th pulse	300	7.5	2250
#8, 3rd pulse	575	2.7	1550
#14, 4th pulse	490	2.5	1225
#21, 1st pulse	750	7	5250

DATA AVAILABILITY (not finished)

All the data used in this study will be available on ZENODO Repository, doi: XXXXXX.

CODE AVAILABILITY (not finished)

References to software tools and codes for this study will be given

REFERENCES

33 Hansen R., Østgaard N., Gjesteland T., Carlson B.. How simulated fluence of photons from Terrestrial Gamma ray flashes at aircraft and balloon altitudes depends on initial parameters. *Journal of Geophysical Research* Vol. 118, Issue 5, pg. 2333-2339, doi: 10.1002/jgra.50143 (2013).

34 Østgaard, N., Balling, J. E., Bjørnsen, T., Brauer, P., Budtz-Jørgensen, C. et al. The Modular X- and Gamma-Ray Sensor (MXGS) of the ASIM Payload on the *International Space Station*, *Space Science Reviews*, **215** (2), article id. 23 (2019).

35 Agostinelli, S., Allison, J., Amako, K., Apostolakis, J., Araujo, H., et al. Geant4—A simulation toolkit. *Nuclear Instruments and Methods in Physics Research Section A: Accelerators, Spectrometers, Detectors and Associated Equipment*, 506(3), 250–303. https://doi.org/10.1016/S0168-9002(03)01368-8 (2003).

36 Chilingarian, A., Amilyan, B., & Vanyan, L. Recovering of the energy spectra of electrons and gamma rays coming from thunderclouds. *Atmospheric Research*, 114–115, 1–16. https://doi.org/10.1016/j.atmosres.2012.05.008 (2012).

37 Lindanger, A., Marisaldi, M., Sarria, D., Østgaard, N., Lehtinen, N., et al. Spectral analysis of individual terrestrial gamma-ray flashes detected by ASIM. *Journal of Geophysical Research* 126(23), e2021JD035347. https://doi.org/10.1029/2021JD035347 (2021).

38 Hauschild, T., & Jentschel, M. Comparison of maximum likelihood estimation and chi-square statistics applied to counting experiments. Nuclear *Instruments and Methods in Physics Research Section A: Accelerators, Spectrometers, Detectors and Associated Equipment*, 457(1–2), 384–401. https://doi.org/10.1016/s0168-9002(00)00756-7 (2001).